

# Mathematical modeling and periodical heat extraction analysis of deep coaxial borehole heat exchanger for space heating

Yaran Wang <sup>a, b</sup>, Yeming Wang <sup>a, b</sup>, Shijun You <sup>a, b</sup>, Xuejing Zheng <sup>a, \*</sup>, Peide Cong <sup>c</sup>,  
Jinkai Shi <sup>c</sup>, Bo Li <sup>c</sup>, Lichuan Wang <sup>c</sup>, Shen Wei <sup>d</sup>

<sup>a</sup> School of Environmental Science and Engineering, Tianjin University, Tianjin 300350, PR China

<sup>b</sup> Key Laboratory of Efficient Utilization of Low and Medium Grade Energy, MOE, Tianjin University, Tianjin 300350, PR China

<sup>c</sup> Tianjin Geothermal Development Co., Ltd., Tianjin 300350, PR China

<sup>d</sup> Faculty of Engineering and Environment, Northumbria University, Newcastle upon Tyne NE1 8ST, UK

\* Corresponding author. Tel.: +086013512419172; fax: +8602227400832. E-mail addresses: zhengxuejing@tju.edu.cn

## Highlights

- ✓ The transient numerical model of coaxial borehole heat exchanger is developed
- ✓ Verification of the proposed model using the operating data from the literature
- ✓ Comparison of the periodical heat extraction and power under 4 operating modes
- ✓ Analysis of the underground temperature distribution transients within 30 days
- ✓ Long-term operation performance of the borehole heat exchanger within 20 years

## Keywords

Numerical model; coaxial borehole heat exchanger; operation strategy; underground temperature distribution transients

## Abstract

The geothermal energy is considered as one of the most promising renewable

techniques for district heating. The deep coaxial borehole heat exchanger (BHE) is an economic and efficient measure for extracting the geothermal energy from underground, which attracts numerous attentions recently. However, the researches on the influences of the operation modes on the periodical heat extraction performances of the deep coaxial BHE are rare. In this paper, an unsteady numerical model of the dynamic operation of the coaxial borehole heat exchanger is established, based on the principles of energy conservation and mass conservation. The proposed model is verified using the operating data from the literature. Space heating of a school building (located at Tianjin, China) is taken as a scenario, and different operation modes during the heating period are simulated and analyzed. Comparisons were carried out on four operating modes: the continuous operation mode, “16+8 mode” (run for 16h and stop for 8h), “12+12 mode” and “8+16 mode”. The recovery of underground temperature distribution during the winter holiday was studied. Results show that, except for the continuous operation mode, the differences between the other three modes on the total extracted heat throughout the whole year and during the 24h within the 90th day are unobvious. Under the “12+12 mode”, when the BHE reaches the stable level, the heat extraction power can be maintained at 301.6 - 528.1kW in the first year, and the decline rate lower than 15% during the 20-year operation period. In addition, at 1 meter from the center of the tube and at depths of 500 meters, 1000 meters, 1500 meters, and 2000 meters, the recovery rates of the underground temperature distribution relative to the initial temperature during the winter vacation are 7.35%, 13.78%, 16.57%, and 17.74%, respectively.

Nomenclature	
$a$	thermal diffusivity ( $\text{m}^2/\text{s}$ )
$D$	diameter (m)
$h$	convective heat transfer coefficient ( $\text{W}/\text{m}^2 \cdot ^\circ\text{C}^{-1}$ )
$M$	the number of control volumes in the radial direction
$m$	mass flow ( $\text{kg}/\text{s}$ )
$N$	the number of control volumes in the depth direction
$r$	distance from center of the BHE (m)
$R$	thermal resistance ( $\text{m} \cdot \text{K}/\text{W}$ )
$t$	time (s)
$T$	temperature ( $^\circ\text{C}$ )
$v$	velocity ( $\text{m}/\text{s}$ )
$y$	depth (m)
$\lambda$	thermal conductivity ( $\text{W}/\text{m} \cdot \text{K}^{-1}$ )
$\rho$	density of water ( $\text{kg}/\text{m}^3$ )
$c_p$	specific heat capacity of water ( $\text{J}/\text{kg} \cdot \text{K}^{-1}$ )
Subscripts	
$B$	backfilling material
$c$	fluid in inner pipe
$ch$	between the fluid in inner pipe and fluid in annular cavity
$ce$	between the fluid in annular cavity and the rock formation
$e$	rock formation
$h$	fluid in annular cavity
$i$	inlet
$in$	inside diameter
$o$	outlet
$out$	outer diameter
1	inner pipe
2	outer pipe

## 1. Introduction

The building energy consumption in China accounts for a relatively large proportion among the total society energy consumption, and the space and domestic heating in the northern region accounts for the largest proportion. Compared with 2015, the China's hot water heat supply increased by 16.5% [1]. In recent years, the construction area in China has continued to grow at a rate of 4 billion square meters per year [2]. In addition, people's requirements for heating quality are increasing. Under this situation, to achieve the two-stage carbon emission reduction goals, China has strived to promote the clean heating techniques. The China's National Energy Administration mentioned in the "Several Opinions on Promoting the Development and Utilization of Geothermal Energy": To steadily promote the mid-deep geothermal energy for district heating [3].

The geothermal energy is considered to be one of the most promising renewable energy resources. Due to the good in heat storage performance of the rock formations, the middle and deep layers of rock and soil can maintain a stable temperature. Other natural renewable resources such as solar energy and wind energy are restricted by factors such as the alternation of day and night, and the change of seasons. Geothermal resources are abundant in reserves, convenient to access, and continuous to utilize.

The form of buried pipe heat exchanger directly affects the effect of geothermal resources. The existing buried pipe heat exchanger mainly includes horizontal and vertical types. Vertical buried pipes are divided into single U-shaped, double U-shaped and coaxial borehole heat exchanger (BHE) [4]. Seokjae Lee et al.[5] evaluated the

thermal performance of the coaxial BHE, geothermal energy showed more stable performance with the coaxial BHE in the ground source heat pump system, than with the single U-shaped buried pipes. The schematic of coaxial BHE is shown in Fig. 1. It has the advantages of small footprint and good heat exchange performance, attracting a large number of researchers on the study of geothermal energy and ground source heat pump systems [6-21].

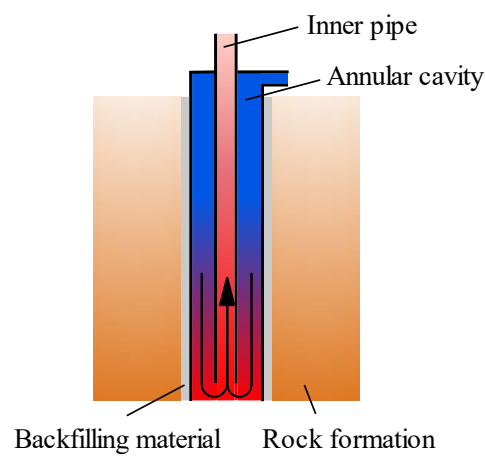


Fig. 1. Diagram of coaxial deep borehole heat exchanger

Modeling the heat transfer process of the coaxial deep borehole heat exchanger is very important for operation analysis. Peng Li et al. [22] established a 3D numerical model for a coaxial deep BHE. Changlong Wang et al. [21] developed a semi-analytical model by considering the geothermal gradient and the heat capacities of different parts of the borehole. They analyzed the 1D radial heat transfer in the grout and the soil based on an analytical solution. However, the solution of 3D numerical model requires a lot of computing resources, on the other hand, 1D numerical model that borehole wall temperature is constant along the depth of ground is considered inaccurate in the application of deep BHE due to the geothermal gradient in deep ground [23]. As the

heat transfer process of the ground are rotational symmetry along the BHE. Hence, using a 2D model to simulate the heat transfer of deep BHE will be efficient.

Henrik Holmberg et al. [24] developed a 2D numerical model to study the coaxial borehole heat exchanger, studied the influence of the flow direction of the mass flow in the range 200-500 m. Zhihua Wang et al. [25] developed a 2D numerical model to examine the effect of the inlet velocity, inlet temperature, flow pattern and pipe diameter on the performance of deep BHE. Liang Fang et al. [26] developed a thermal analysis software package, which is based on the finite difference method, presented the relations of the nominal deep BHE capacity to its key parameters such as the borehole depth, geothermal heat flux and thermal conductivity of subsurface. Xianzhi Song et al. [20] established an unsteady-state heat transfer model for a coaxial deep BHE, comprehensively analyzed the effects of key factors on the coaxial BHE performance and verified the sustainability of coaxial BHE system. Jun Liu et al. [27] proposed a numerical model considering the comprehensive effects of geothermal gradients and heat loss from inner pipe, analyzed the influence of flow rate on heat loss. Yibin Huang et al. [28] analyzed and discussed the effects of the heat load mode, flow rate, heat load, radius ratio and soil thermal conductivity on the fluid and soil. Yongqiang Luo et al. [29] analyzed the influence of pipe sizing ratio, inlet thermal flow rate and initial soil temperature distribution. Kaituo Jiao et al. [19] proposed an analytical model for the BHE based on the moving finite line source model to analyze the long-term heat transfer performance, and verified the impact of the groundwater flow is small in local heat flux. It is obviously that most of the existing research focuses

on the optimization of heat exchanger performance.

The development of mid-deep geothermal energy heating has been promoted as a solution to meet district heating in part; researchers have proposed fast algorithms and factors that affect the heat transfer performance of BHE. However, when applied to district heating, the performances of the BHE under different periodical operation modes should be properly evaluated. Wanlong Cai et al. [30] compared and analyzed the changes of outlet water temperature in the four modes. However, the amount of heat extraction is more meaningful for space heating. In addition, the model established by the previous study focuses on the operation period, when the intermittent operation of the BHE is considered, natural convection currents which dominate over vertical heat conduction is very important for the temperature recovery during the shut-in period [31]. In this study, a 2D numerical model which considers the heat conduction of the fluid is established. Besides, the space heating of a school building (winter vacation during heating period) in Tianjin, China, is taken as a scenario. Different operation modes of the coaxial BHE are evaluated. By comparing the heat extraction effects of different operating strategies, reasonable suggestions for the use of geothermal resources are put forward.

## **2. Modeling**

### *2.1 Physical model*

The heat transfer process involves three parts: heat exchange outside the well, at the boundary of BHE, and inside the BHE. The heat exchange outside the BHE includes

heat conduction of rock formation and backfilling material; heat exchange at the boundary includes heat conduction on the outer pipe wall of the BHE and convective heat exchange with the circulating fluid in the annular cavity; heat exchange in the BHE includes convective heat transfer and heat conduction of fluid in the BHE (including fluid in inner pipe and the annular cavity) and its convective heat transfer with the inner pipe wall, inner pipe wall heat conduction.

The 3D heat transfer problem is simplified as the two-dimensional heat transfer problem in the radial and depth directions, as shown in Fig. 2. The following simplifications were considered when constructing the model: (1) Regarding the rock formation and backfill material as media with uniform texture, isotropy and constant physical parameters; (2) Ignore the influence of water content on the heat transfer process, only consider the heat conduction of the underground rock formations; (3) The underground rock formations are considered in close contact with no contact thermal resistance; (4) The inlet temperature of the inner pipe is equal to the outlet temperature of the annular cavity at the bottom of the borehole; (5) The radius of the heat exchanger is very small relative to the radius of the rock formation, the temperature gradient of the circulating fluid in the annular cavity and the inner pipe in the radial direction is neglected, hence, only the temperature change of the circulating fluid in the depth direction is considered.



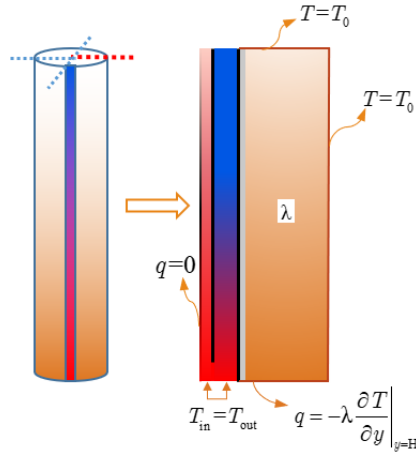


Fig. 2 Physical model

## 2.2 Mathematical model

The energy conservation equation of the rock formation heat conduction process can be written as:

$$\frac{\partial T_e}{\partial t} = \frac{a_e}{r} \frac{\partial T_e}{\partial r} + a_e \left( \frac{\partial^2 T_e}{\partial r^2} + \frac{\partial^2 T_e}{\partial y^2} \right) \quad (1)$$

where  $T_e$  and  $a_e$  are temperature and thermal diffusivity of the rock formation;  $t$  is time;  $r$  is distance between the control volume and tube center;  $y$  is depth.

The thermal fluid (fluid in inner pipe) energy conservation equation can be written as:

$$\frac{\partial T_h}{\partial t} - v_h \frac{\partial T_h}{\partial y} = a_h \frac{\partial^2 T_h}{\partial y^2} + \frac{4(T_c - T_h)}{\pi \rho c_p D_{h,in}^2 R_{ch}} \quad (2)$$

where  $T_h$  and  $T_c$  are temperature of the thermal fluid and cold fluid;  $v_h$  and  $a_h$  is the flow velocity and the thermal diffusivity of the thermal fluid;  $D_{h,in}$  and  $D_{h,out}$  are inner diameter and outer diameter of the inner pipe;  $h_h$  and  $h_c$  are convection heat transfer coefficient of the fluid in inner pipe and inner wall of inner pipe and the fluid in annular cavity and outer wall of inner pipe;  $R_{ch}$  is the thermal resistance between the fluid in inner pipe and the annular cavity:

$$R_{ch} = \frac{1}{\pi D_{h,in} h_h} + \frac{1}{2\pi\lambda_1} \ln \frac{D_{h,out}}{D_{h,in}} + \frac{1}{\pi D_{h,out} h_c} \quad (3)$$

where  $\lambda_1$  is the thermal conductivity of inner tube.

The cold fluid (fluid in annular cavity) energy conservation equation can be written as:

$$\frac{\partial T_c}{\partial t} + v_c \frac{\partial T_c}{\partial y} = a_c \frac{\partial^2 T_c}{\partial y^2} + \frac{4(T_h - T_c)}{\pi(D_{c,in}^2 - D_{h,out}^2)\rho c_p R_{ch}} - \frac{4(T_c - T_e)}{\pi(D_{c,in}^2 - D_{h,out}^2)\rho c_p R_{ce}} \quad (4)$$

where  $v_c$  and  $a_c$  is the flow velocity and the thermal diffusivity of the cold fluid;  $D_{c, in}$  and  $D_{c,out}$  are inner diameter and outer diameter of the outer pipe;  $D_{B, in}$ ,  $D_{B, out}$  are inner diameter and outer diameter of the backfilling material;  $h_c$  is the convection heat transfer coefficient of the fluid at the interface of the annular cavity and inner wall of the outer pipe;  $R_{ce}$  is the thermal resistance between the fluid in annular cavity and the borehole wall :

$$R_{ce} = \frac{1}{\pi D_{c,in} h'_c} + \frac{1}{2\pi\lambda_2} \ln \frac{D_{c,out}}{D_{c,in}} + \frac{1}{2\pi\lambda_B} \ln \frac{D_{B,out}}{D_{B,in}} \quad (5)$$

where  $\lambda_2$  and  $\lambda_B$  are the thermal conductivity of the outer tube and backfilling material.

The boundary conditions on the top and right boundaries of the underground are the first type of boundary conditions, which are maintained as the initial temperature distribution (12°C of the top boundary, and constant temperature gradient of the right boundary with 0.025°C/m, as the depth increases). Ref. [20] shows that the influence radius on the underground temperature distribution during the first-year operation is 10m. In addition, related research has shown that long-term thermal performance of deep coaxial BHE is relatively stable, its heat output capacity has not changed much in 20 years [28]. This paper studies the operation of the BHE for the first year, hence the

calculated radius of 10m is adopted.

The second type of boundary condition is considered for the bottom boundary, which can be described as Eq. (5); the third type of boundary condition is adopted for the interface of the rock formation and the borehole (the borehole wall in Fig. 3), described by Eq. (6):

$$\frac{\partial T_e}{\partial y} = \frac{\partial T_e}{\partial y} \Big|_{t=0} \quad (5)$$

$$q_w = \frac{T_c - T_e}{R_{ce}} \quad (6)$$

where  $q_w$  is the heat flux density at the left boundary of the underground.

The initial flow velocity of the circulating fluid is 0m/s, and the temperature is the same as the underground temperature distribution along the depth direction. The initial temperature distribution is:

$$T(i) = T_{sur} + \left[ \frac{1}{2} + (i-1) \right] dy \frac{\partial T_e}{\partial y} \Big|_{t=0} \quad (7)$$

where  $i$  is the layer of discrete points,  $1 \leq i \leq M$ ;  $M$  is the number of layers of the control volume divided in the depth direction;  $dy$  is the distance between adjacent discrete points in the depth direction.

### 2.3 Discretized model

The rock formation energy conservation equation is discretized between two half time steps in the alternate direction implicit scheme; the convection term of fluid energy conservation is discretized as the first-order implicit upwind scheme, and the heat conduction term is discretized as the second-order precision difference scheme. The internal node method is used to discretize the aforementioned equations in the solution

space, and the discretization method is shown in Fig. 3. Besides, different time steps are considered, a longer time step is used for the discretization of the underground energy conservation equation.

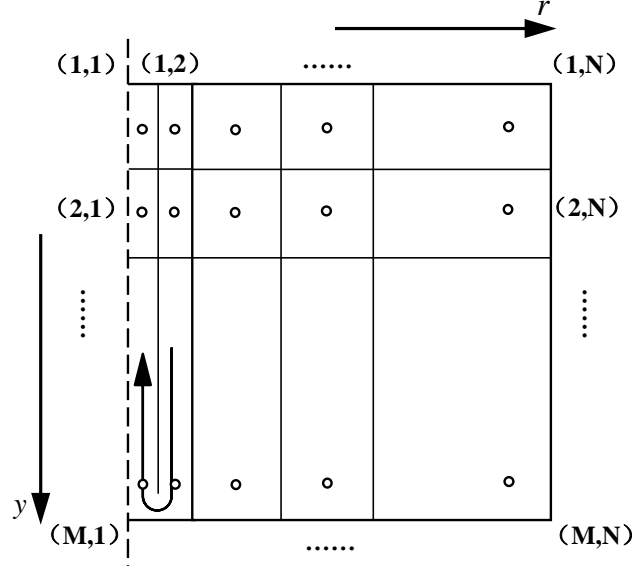


Fig. 3 Spatial discretization with inner node method

The discrete equation for the underground heat conduction in the first half time step is expressed as:

$$A_{i,j-1}T_{i,j-1}^{n-\frac{1}{2}} + A_{i,j}T_{i,j}^{n-\frac{1}{2}} + A_{i,j+1}T_{i,j+1}^{n-\frac{1}{2}} = B_{i-1,j}T_{i-1,j}^{n-1} + B_{i,j}T_{i,j}^{n-1} + B_{i+1,j}T_{i+1,j}^{n-1} \quad (8)$$

where

$$A_{i,j-1} = -\frac{a_e}{\Delta r^2} + \frac{a_e}{2r_j\Delta r}; \quad A_{i,j} = \frac{2}{\Delta t} + \frac{2a_e}{\Delta r^2}; \quad A_{i,j+1} = -\frac{a_e}{\Delta r^2} - \frac{a_e}{2r_j\Delta r};$$

$$B_{i-1,j} = B_{i+1,j} = \frac{a_e}{\Delta y^2}; \quad B_{i,j} = \frac{2}{\Delta t} - \frac{2a_e}{\Delta y^2}$$

where  $r_j$  is the distance from the  $j$ th control volume to the center of the BHE,  $1 \leq j \leq N$ .

The discrete equation for the model of rock formations in the second half time step is expressed as:

$$A'_{i-1,j}T_{i-1,j}^n + A'_{i,j}T_{i,j}^n + A'_{i+1,j}T_{i+1,j}^n = B'_{i,j-1}T_{i,j-1}^{n-\frac{1}{2}} + B'_{i,j}T_{i,j}^{n-\frac{1}{2}} + B'_{i,j+1}T_{i,j+1}^{n-\frac{1}{2}} \quad (9)$$

where

$$A'_{i-1,j} = -\frac{a_e}{\Delta y^2}; \quad A'_{i,j} = \frac{2}{\Delta t} + \frac{2a_e}{\Delta y^2}; \quad A'_{i+1,j} = -\frac{a_e}{\Delta y^2};$$

$$B'_{i,j-1} = \frac{a_e}{\Delta r^2} - \frac{a_e}{2r_j \Delta r}; \quad B'_{i,j} = \frac{2}{\Delta t} - \frac{2a_e}{\Delta r^2}; \quad B'_{i,j+1} = \frac{a_e}{2r_j \Delta r} + \frac{a_e}{\Delta r^2}$$

The discrete equation for the model of the fluid in inner pipe is expressed as:

$$A_{h,i-1}T_{h,i-1}^n + A_{h,i}T_{h,i}^n + A_{h,i+1}T_{h,i+1}^n = BT_{h,i}^{n-1} + A_{h,c,i}T_{c,i}^{n-1} \quad (10)$$

where

$$A_{h,i-1} = -\frac{a_h}{\Delta y^2}, \quad A_{h,i} = \frac{1}{\Delta t} + \frac{v_h}{\Delta y} + \frac{2a_h}{\Delta y^2} + \frac{4}{\pi \rho_c D_{h,in}^2 R_{ch}},$$

$$A_{h,i+1} = -\frac{v_h}{\Delta y} - \frac{a_h}{\Delta y^2}, \quad A_{h,c,i} = \frac{4}{\pi \rho_c D_{h,in}^2 R_{ch}}, \quad B = \frac{1}{\Delta t}$$

The discrete equation for the model of the fluid in annular cavity is expressed as:

$$A_{c,i-1}T_{c,i-1}^n + A_{c,i}T_{c,i}^n + A_{c,i+1}T_{c,i+1}^n = BT_{c,i}^{n-1} + A_{c,i,l}T_{i,l}^{n-1} + A_{c,h,i}T_{h,i}^{n-1} \quad (11)$$

where

$$A_{c,i-1} = -\frac{a_c}{\Delta y^2} - \frac{v_c}{\Delta y},$$

$$A_{c,i} = \frac{1}{\Delta t} + \frac{v_c}{\Delta y} + \frac{2a_c}{\Delta y^2} + \frac{4}{\pi(D_{c,in}^2 - D_{h,out}^2)\rho_c R_{ch}} + \frac{4}{\pi(D_{c,in}^2 - D_{h,out}^2)\rho_c R_{ce}}$$

$$A_{c,i+1} = -\frac{a_c}{\Delta y^2}, \quad A_{c,h,i} = \frac{4}{\pi(D_{c,in}^2 - D_{h,out}^2)\rho_c R_{ch}}, \quad A_{c,i,l} = \frac{4}{\pi(D_{c,in}^2 - D_{h,out}^2)\rho_c R_{ce}}$$

### 3. Model verification

#### 3.1 Validation by experimental data

To verify the accuracy of the model, open experimental data reported in Ref. [32] are adopted. Geometric and physical parameters of the case are shown in Table 1.

Table 1. Geometric and physical parameters of the case

Description	Symbol	Value	Unit
Borehole depth	$Y$	880	m
Outer diameter of outer pipe	$D_{c,out}$	17.78	cm
Inner diameter of outer pipe	$D_{h,out}$	16.88	cm
Outer diameter of inner pipe	$D_{c,in}$	8.90	cm
Inner diameter of inner pipe	$D_{h,in}$	6.98	cm
Thermal diffusivity of rock-soil	$a_e$	$6.03 \times 10^{-7}$	$m^2/s$
Thermal conductivity of outer pipe	$\lambda_c$	46.1	$W/m \cdot K^{-1}$
Thermal conductivity of inner pipe	$\lambda_h$	0.02	$W/m \cdot K^{-1}$
Ground surface temperature	$T_{sur}$	30	$^{\circ}C$
Flow rates	--	4.8	$m^3/h$
Geothermal gradient	--	1 (<300m)	K/100m
		13 ( $\geq 300m$ )	

The comparison between the simulated and experimental results the inner tube outlet temperatures are shown in Fig. 4. The relative errors of the outlet temperature between the simulated and experimental results are all within 10%. When the BHE operates at stable state, the relative errors are within 5%. The results indicate that the proposed numerical model is satisfactory for simulating the underground heat exchange process of the deep coaxial BHE.

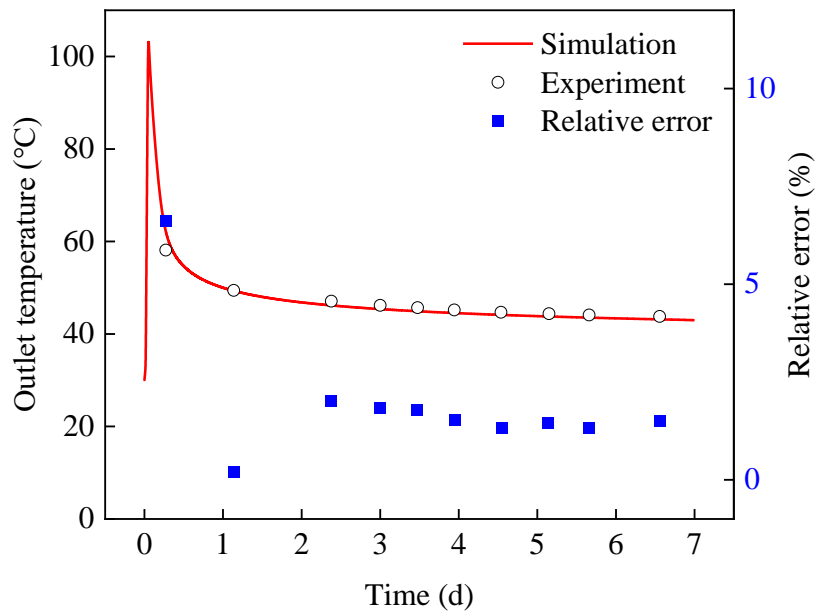


Fig 4. Comparison between simulation result and experiment data

### 3.2 Verification of grid independence

To ensure the accuracy of the numerical model, it is necessary to test the independence of the grid. The uniform grid is utilized for the numerical model, and the independence of the axial step length ( $\Delta z$ ), radial step length ( $\Delta r$ ) and discrete time step of the underground ( $\Delta t_e$ ) and fluid ( $\Delta t_w$ ) energy conservation equation involved in Eq. (1), Eq. (2) and Eq. (4) are analyzed and shown in the Fig. 5.

As shown in Fig.5,  $\Delta r$  has the most significant influence on the simulation results (Fig. 5d). When  $\Delta r$  is less than 0.4 m, the simulation result changes very little, so  $\Delta r$  is selected as 0.4m.  $\Delta y$  (Fig. 5a),  $\Delta t_w$  (Fig. 5b) and  $\Delta t_e$  (Fig. 5c) have little influence on the simulation results. Considering the accuracy and calculation speed of the model,  $\Delta y$ ,  $\Delta t_w$ ,  $\Delta t_e$  and  $\Delta r$  is set as 10 m, 60 s, 300 s and 0.4 m, respectively.

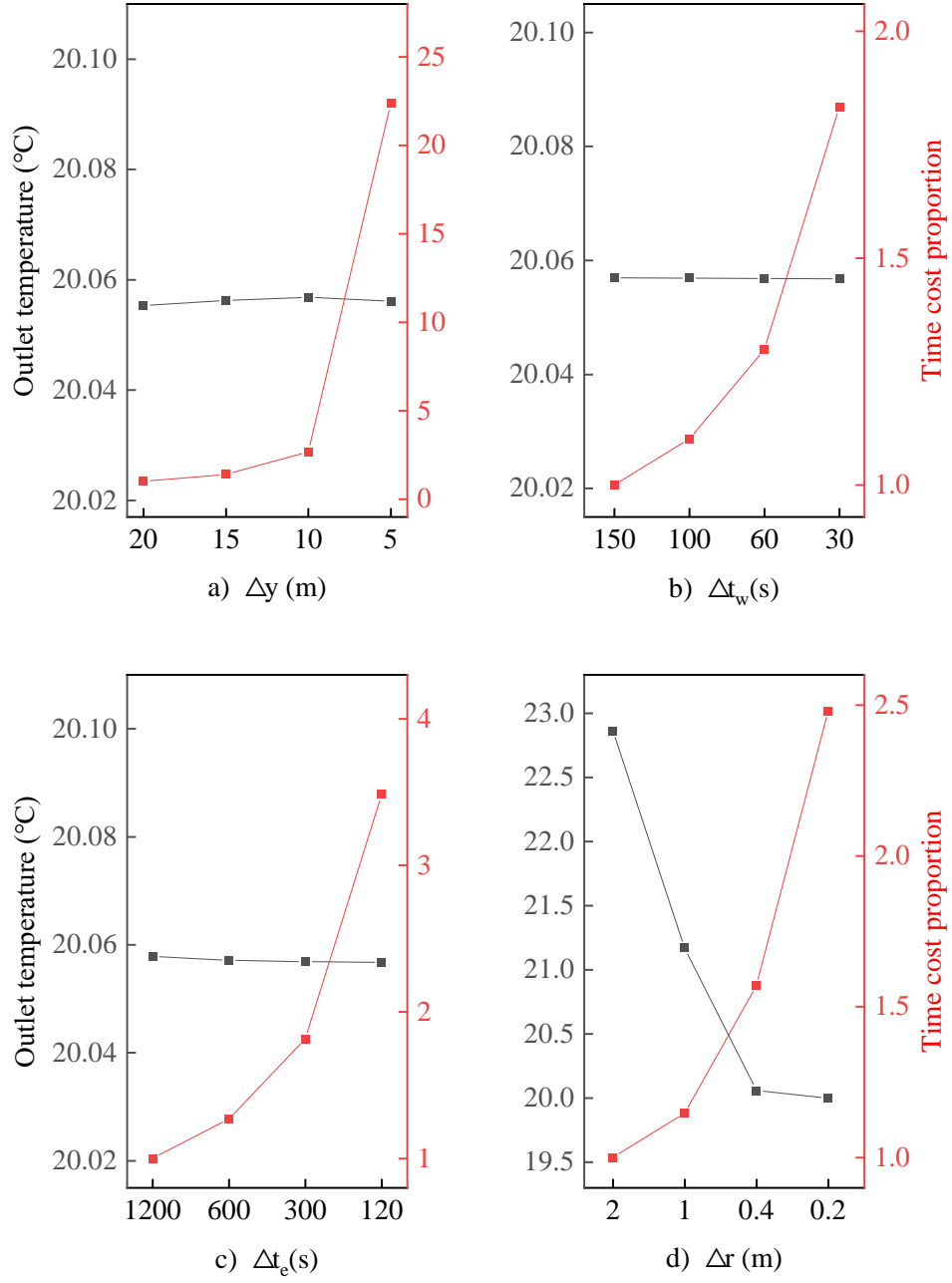


Fig.5 Grid independence tests of the model

## 4. Results and Discussion

### 4.1 Case study

A school building heating project to be located in Tianjin (China) is taken as the case study of the deep coaxial BHE operation performances, and the heating will be stopped during the winter vacation (30 days). The heating period is from November 1st



to March 30th. The calculation period is set to 150 days. The depth and diameter of the borehole are 2400m and 0.241m respectively, which adopts a coaxial BHE, with a design circulating water flow rate of 30m<sup>3</sup>/h, injected from the annular cavity, and flows out from the inner pipe after absorbing heat in the well. The heat is extracted by an electric heat pump, and the temperature of the injected temperature is maintained as a constant value. The deep coaxial BHE and the heat pump undertakes the base heating load, and a gas boiler undertakes the peak load. The extracted geothermal heat is adequately utilized in priority for heating, and the peak load is compensated by a gas boiler.

Table 2 lists the physical parameters of the heat conduction medium. Based on the geological data of the Tianjin geothermal reservoir, the ground surface temperature is 12°C, and the geothermal gradient is 0.025°C/m. In this study, outer pipe with an outer diameter of 177.8 mm and a wall thickness of 9 mm were used. The inner pipe had an outer diameter of 112.4 mm and a wall thickness of 11.2 mm. Moreover, a boundary condition of constant inlet temperature (15°C, 18°C and 20°C) is utilized, the heat output capability is utilized as the index to compare the performance of the heat exchanger under different operating modes.

Table 2. Physical parameters of heat conduction medium

Physical parameters	Outer pipe	Backfilling material	Formation	Inner pipe	Water
Density (kg/m <sup>3</sup> )	--	2140	1925	--	998
Thermal capacity (J/(kg·°C))	--	2000	1040	--	4200
Thermal conductivity (W/(m·°C))	45	0.7	3	0.3	0.61

#### 4.2 Operation mode analysis

The performance of the coaxial BHE during a heating period was simulated in the following operating modes:

- 1) Continuous operation mode, running 24 hours a day;
- 2) “16+8 mode”, run 16 hours then stop for 8 hours a day;
- 3) “12+12 mode”, run 12 hours then stop for 12 hours a day;
- 4) “8+16 mode”, run 8 hours then stop for 16 hours a day.

The heat extraction power and outlet temperature are two indicators to evaluate the performance of the BHE in this study. The heat extraction power is calculated by the following formula:

$$P = c_p m (T_o - T_{in}) \quad (8)$$

The performance of the BHE in continuous operation is shown in Fig. 6. As shown in Fig. 6(a), it is indicated that at the beginning of the operation, the heat extraction power can reach a peak value of about 1600 kW, then the heat extraction power sharply decreases; after about 10 days of operation, the heat extraction power changes greatly reduced; after about 30 days of operation, the heat extraction power is basically stable at about 200kW. The heat extraction power reaches the sub-peak value of about 1200kW after winter vacation. The change of the heat taken after that is similar to the initial stage of operation, and finally stabilizes at about 200kW. In addition, it is indicated that the heating extraction power increases as the inlet temperature decreases in the range of 15 - 18°C. The change trend of the outlet temperature over time in Fig.6(b) is similar to that of heat extraction power. The outlet temperature can be

stabilized at around 21.3°C, 23.6°C, 25.2°C respectively when the inlet temperature is 15°C, 18°C and 20°C.

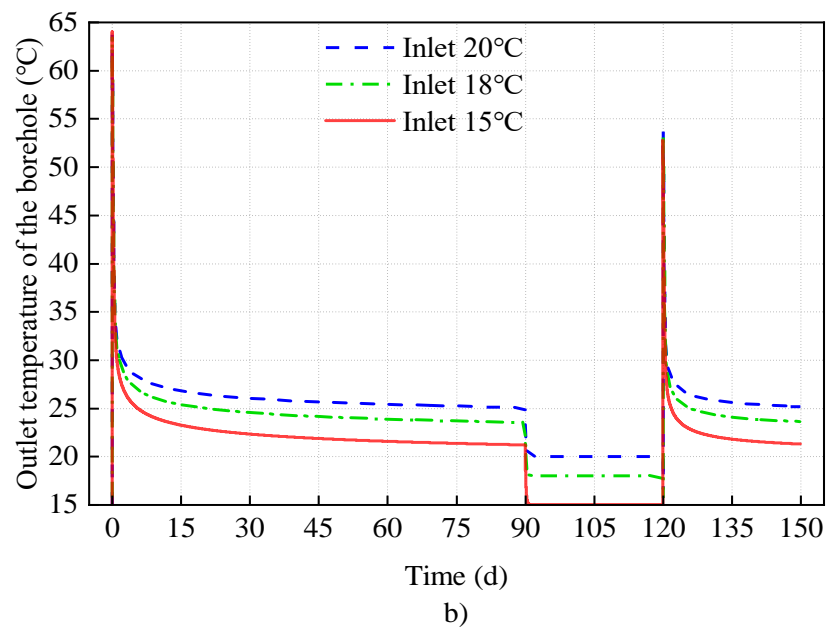
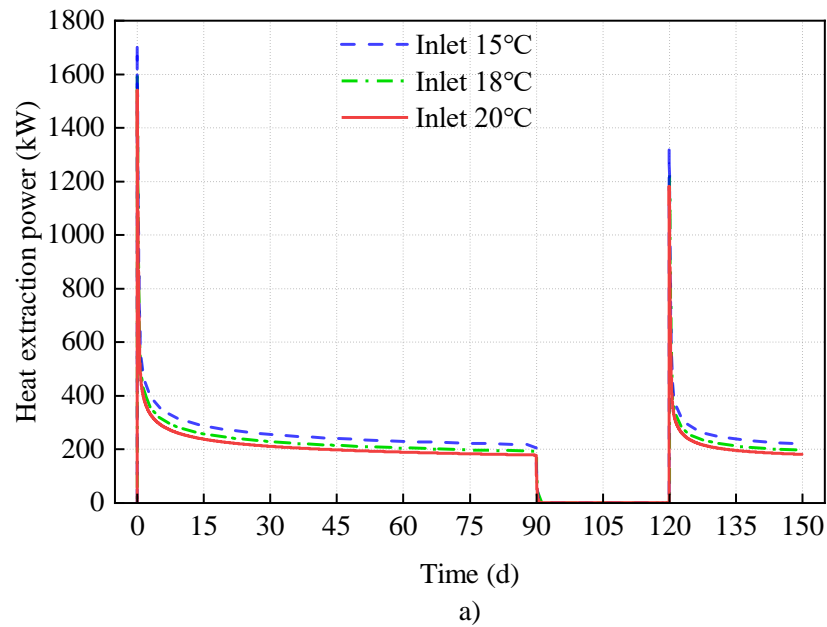
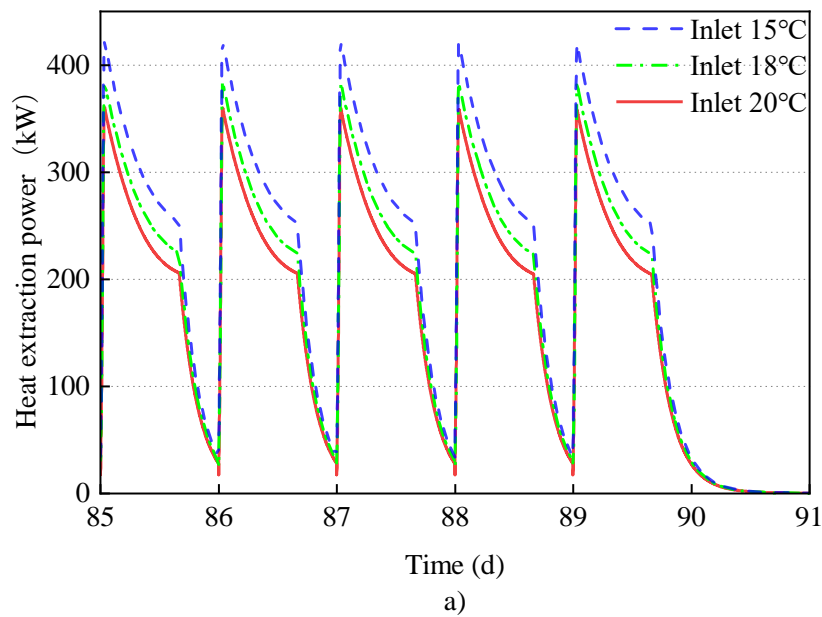


Fig.6 The performance of the BHE in continuous operation

Considering that the duration of the heat extraction power remains at the peak for a short period of time, and only stable heat output is of reference to an actual project. Hence, the situation when the BHE is running stably (the 86th to 90th day) is taken as

an example to observe the performance of the BHE in the “16+8 mode”. Fig. 7(a) shows that when the inlet water temperature is 15°C, 18°C, and 20°C, on about the 50th minute after the system is turned on in each day, the heat extraction power will reach the peak value of 420kW, 380kW, and 360kW, respectively. After that, the heat extraction power begins to decrease until the system stops running. Then the heat extraction power will reduce to about 250kW, 220kW, and 205kW respectively. As is the same with the continuous operation mode, with the inlet temperature decreasing, the heat extraction power increases. In addition, it can be found that the heating power dropped to 0 before the end of the 91st day, which indicates that the fluid at the outlet of the inner tube and the inlet of the annular cavity has undergone sufficient heat exchange and reached the same temperature, as shown in Fig. 7(b). Fig. 7(b) shows that the temperature difference between inlet and outlet can be maintained at 7°C at the end of the operation on day 86 – 90 when the inlet temperature is 15°C, that of about 6°C when the inlet temperature is 18°C and 20°C.



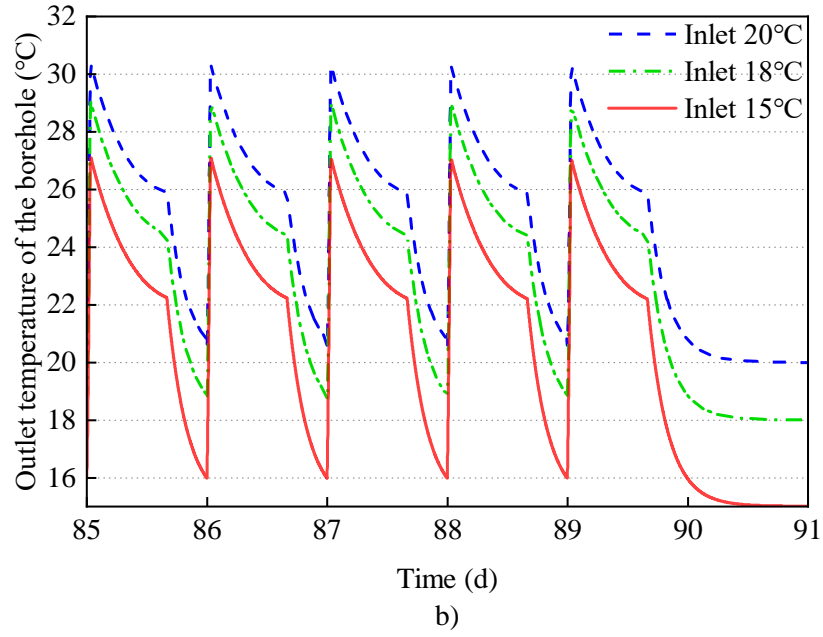


Fig.7 The performance of the BHE in “16+8 mode”

Fig. 8 shows the performance of the BHE from the 86th to 90th day in “12+12 mode”. Fig. 8(a) shows that when the inlet water temperature is 15°C, 18°C, and 20°C, the heat extraction power can reach the peak value of 530kW, 490kW, and 460kW on about the 50th minute after the system is turned on in each day. After that, the heat extraction power will reduce to about 300kW, 265kW, and 245kW respectively until the system stops running. Fig. 8(b) shows that the temperature difference between inlet and outlet can be maintained at 9°C at the end of the operation on day 86 – 90 when the inlet temperature is 15°C, that of about 8°C and 7°C respectively when the inlet temperature is 18°C and 20°C. Until it stops running, the rate of decline of the heat extraction power begins to decrease significantly. Hence, it can be inferred that the BHE can maintain high power output within 12 hours of running time.

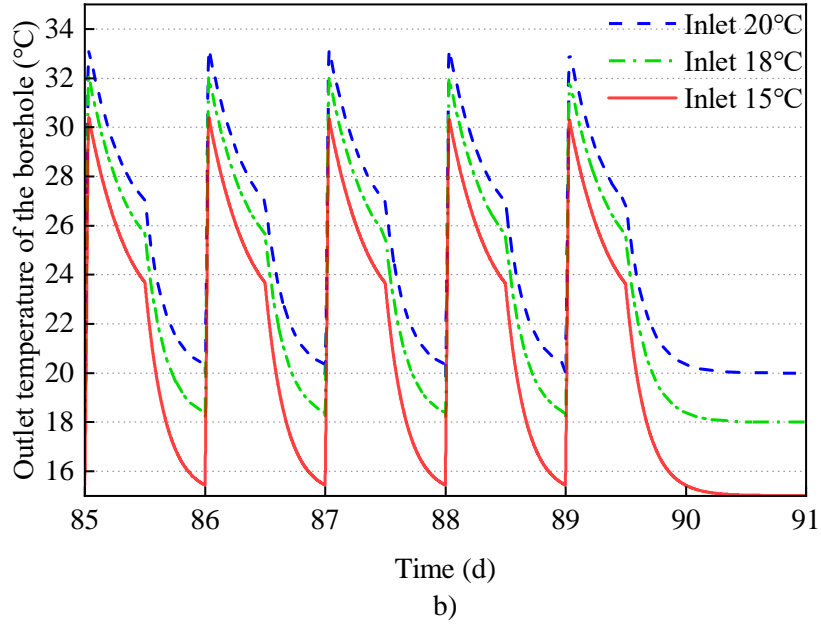
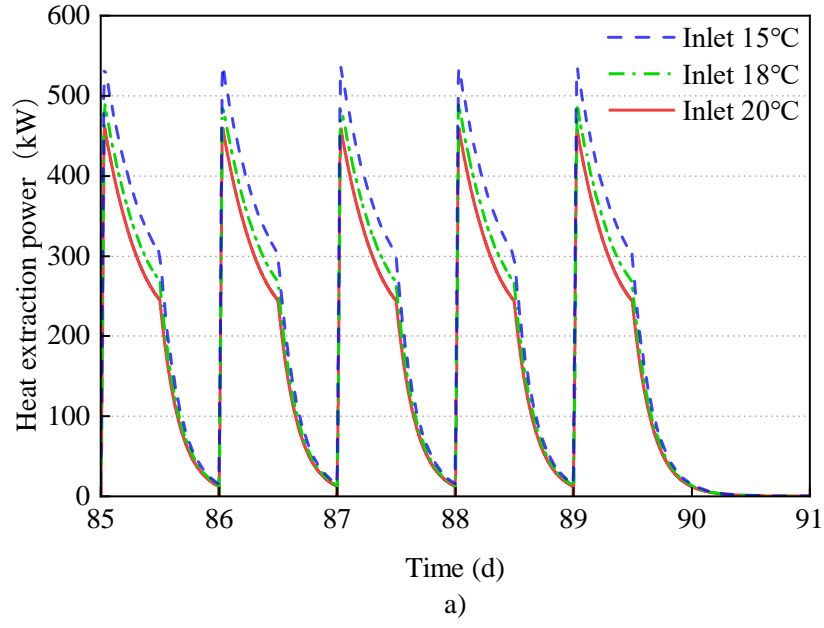


Fig.8 The performance of the BHE in “12+12 mode”

Fig. 9 shows the performance of the BHE from day 86 to 90 in “8+16 mode”. Fig. 9(a) shows that when the inlet water temperature is 15°C, 18°C, and 20°C, the heat extraction power reaches the peak value of 700kW, 636kW, and 600kW on about the 50th minute after the system is turned on in each day. After that, the heat extraction power will reduce to around 420kW, 375kW, and 340kW, respectively, until the system

stops running. Fig. 9(b) shows that the temperature difference between the inlet and outlet is greater than that in “16+8 mode” and “12+12 mode” at the end of the 86-90th day. However, the heat extraction power and the outlet temperature are still falling rapidly, with a large slope until it stops running, which is indicated that the 8-hour run time is too short to extract more heat.

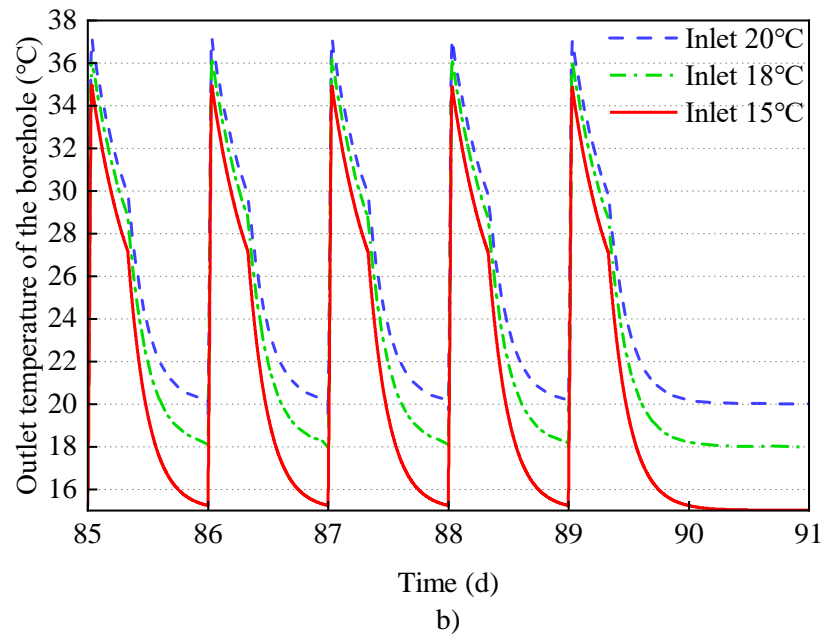
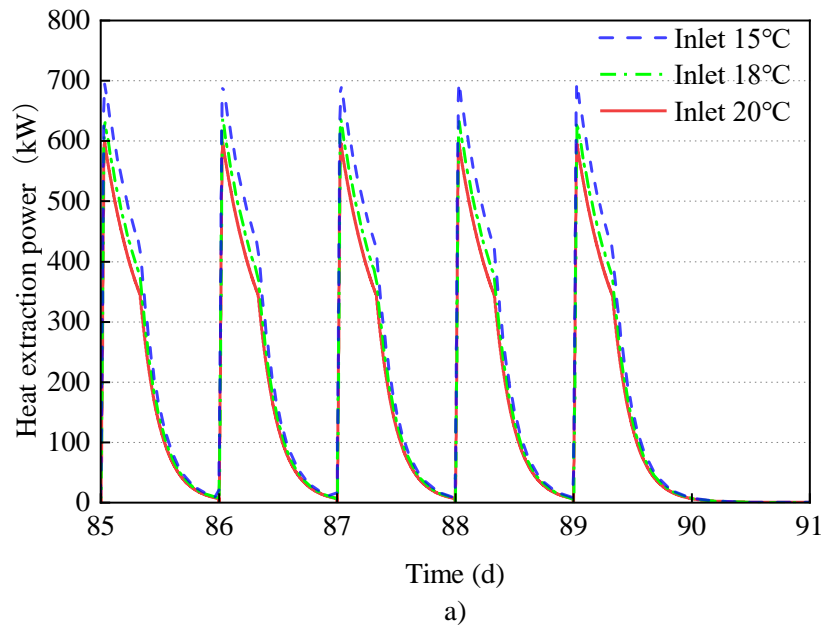


Fig.9 The performance of the BHE in “8+16 mode”

As shown in Fig. 10, taking the 90th day of each operation mode for quantitative analysis, it can be concluded that compared with the continuous operation mode, the heat extraction power under the “8+16 mode” has been greatly improved. When the inlet water temperature is 15°C, the heat extraction power could reach 422.0 kW when the system stops running, and on the same day the peak value during operation can reach 693.8kW, however, this mode runs for a short period of time in each day, and the 8-hour run time is too short to extract more heat. Compared with continuous operation mode, the increase in heat extraction power in “16+8 mode” is less. When the "12+12 mode" operates stably, the daily heat extraction power range is 301.6 - 528.1kW. When the heat load index is 80W/m<sup>2</sup>, the heat power can cover a the heating load of 4524.00 - 7921.50 m<sup>2</sup> building area (with the heat pump COP = 5). In addition, the “12 + 12 mode” is suitable for buildings with regular changes between day and night in heating load (such as school and office buildings).



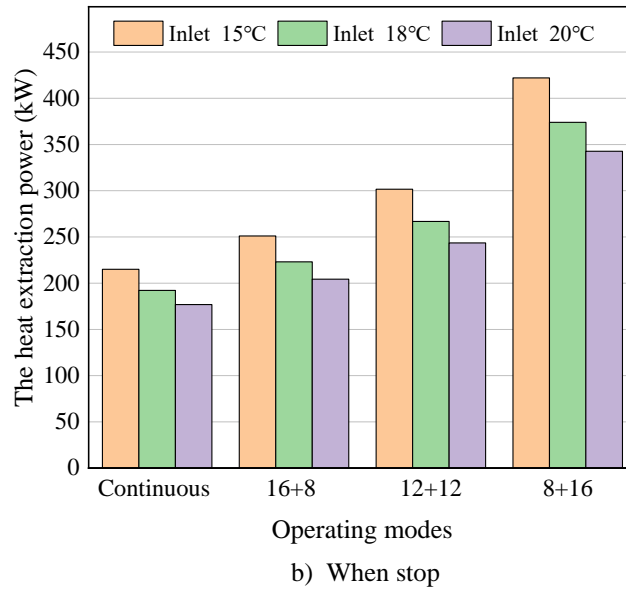
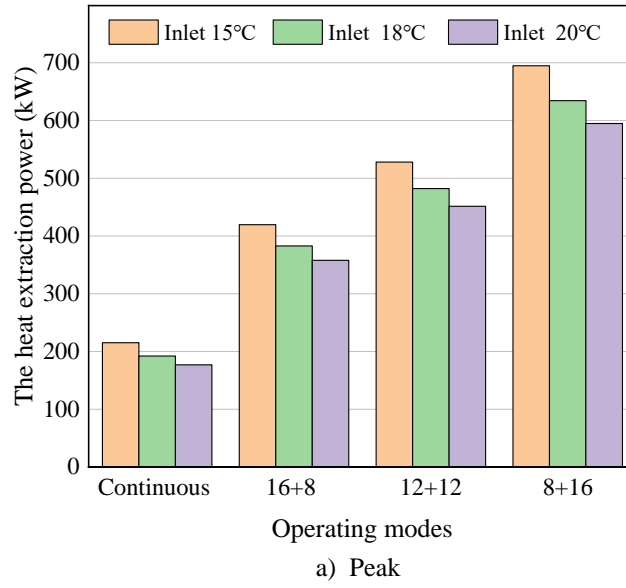


Fig.10 Performance of each operating mode on the 90th day

Fig. 11 shows the annual heat extraction (heating period for 150 days and stop heating for 30 days on 91th day) in each operating mode. It is indicated that when the inlet temperature is the same, the differences of the annual heat extraction for each working condition are not obvious. As an example, for the inlet temperature of 15°C, the annual heat extraction under “12+12 mode” is 2932.8 GJ, which is 212.1 GJ more than the continuous operation mode, and the increase ratio is 7.80%. Besides, the annual

heat extractions under the “16+8 mode”, “12+12 mode” and “8+16 mode” differ by less than 1%. However, the inlet temperature has a significant influence on the annual heat extraction in the same mode. When the inlet temperature is 15°C, 18°C, and 20 °C respectively, the annual heat extraction is 2932.8 GJ, 2627.4 GJ and 2423.7 GJ in the “12+12 mode”. Therefore, it is effective to reduce the inlet temperature from the perspective of annual heat extraction. This is because the fluid in the annular cavity heat to the rock formation when it flows through the shallow rock formation with lower temperature. The higher the inlet temperature, the stronger the heat exchange process and the greater the heat loss. Therefore, lowering the inlet temperature is beneficial to increase the heat extraction power.

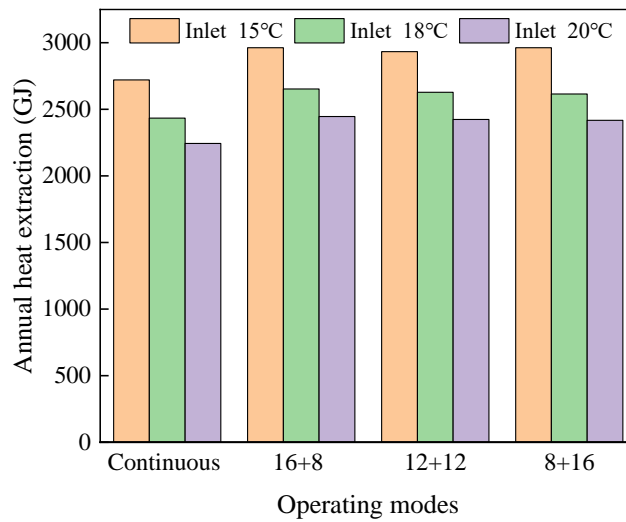


Fig.11 Annual heat extraction of each operating mode

Fig. 12 shows the heat extraction on the 90th day of each operating mode. The situation is similar to Fig. 11. Take the inlet temperature of 18°C as an example, the heat extraction on the day in “12+12 mode” is 18.57 GJ, which is 1.87 GJ more than the continuous operation mode, and the increase ratio is 11.18%. The heat extractions

on the days under the “16+8 mode”, “12+12 mode” and “8+16 mode” have little difference. When the inlet temperature is 15°C, 18°C, and 20 °C, respectively, the heat extractions on the 90th day are 20.76 GJ, 18.57 GJ and 17.10 GJ under the “12+12 mode”. Hence, it is also effective to reduce the inlet temperature from the perspective of daily heat extraction when the BHE runs stably.

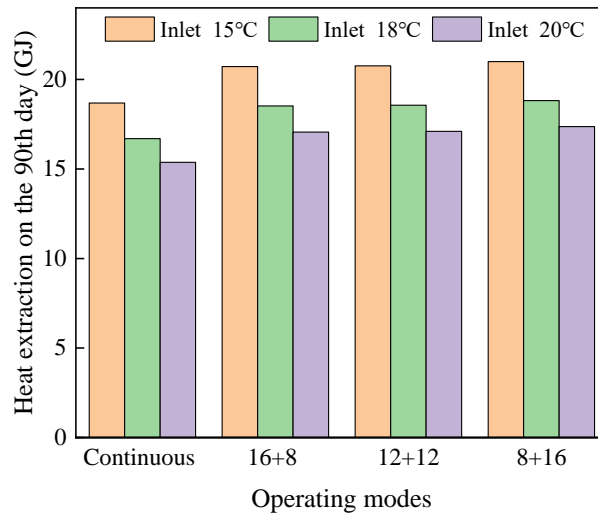


Fig.12 Heat extraction on the 90th day of each operating mode

#### 4.3 Temperature recovery analysis

In order to observe the recovery of the rock formations during the shutdown of the system, for an analysis of the winter vacation for 30 days, Fig. 12 shows the temperature distribution of the underground before and after the holiday in “12+12 mode”. It is indicated that near the BHE, with the increase of depth, the temperature is more difficult to recover. This is because of that the temperature distribution of the deeper rock formations is deteriorated more seriously during operation. In addition, from Fig.12(a), it can be found that the shallow surface underground is heated during the operation of BHE, which proves that the circulating fluid has lost heat.

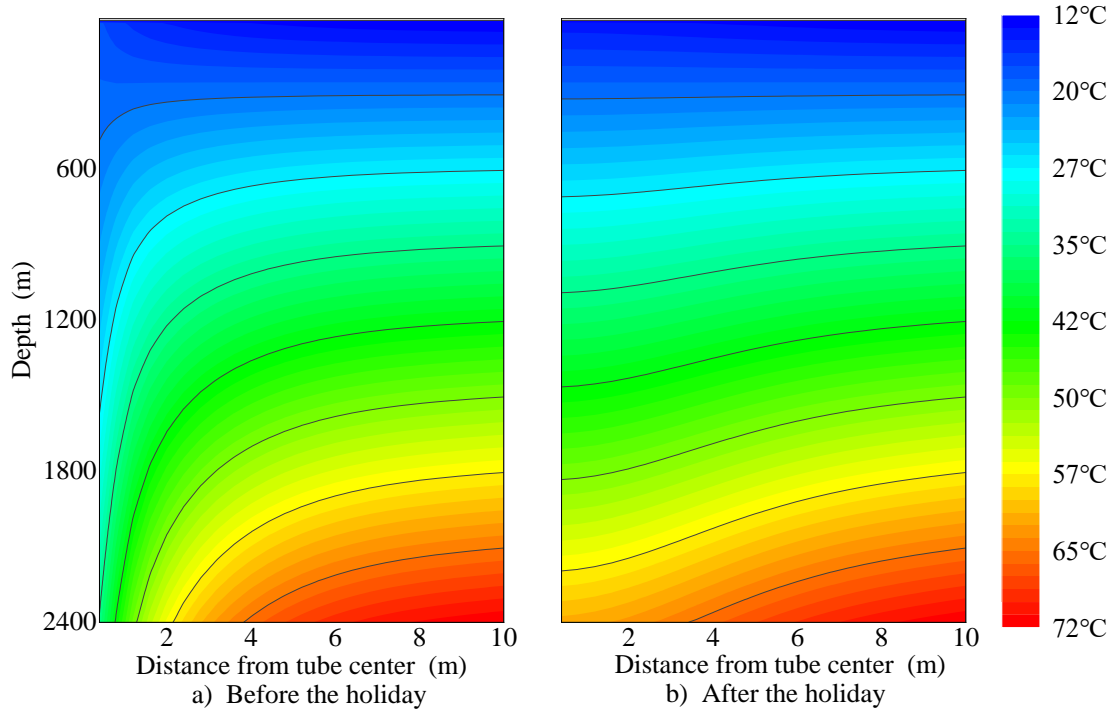


Fig.13 Rock formation temperature distribution in the first year

Specifically, take the temperature of the rock formation control volume at the distance of 1 meter from the center of the tube and a depth of 500 meters, 1000 meters, 1500 meters, and 2000 meters for analysis. The temperature change of the rock formation control volume during the heating period is shown in Fig. 13. It is indicated that during the operation of the BHE, the temperature fluctuations increase with the increase in depth. During the winter vacation, the recovery degree of the underground temperature distribution also increases with the increase in depth. At depths of 500 meters, 1000 m, 1500 m, and 2000 m, within 30 days, the underground temperature recovered 1.8°C, 5.1°C, 8.2°C, and 11°C, respectively. Relative to the initial temperature of each control volume, the recovery ratios were 90.77%, 82.57%, 79.49%, and 78.37%, respectively. It is indicated that the temperature of the rock formation cannot be completely restored to the initial state within the 30-day recovery period.

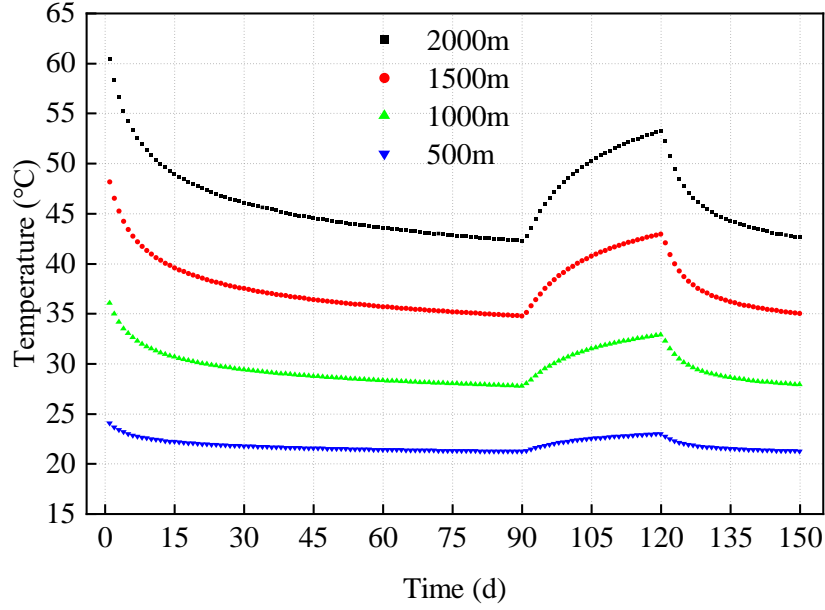


Fig.14 Temperature change of the rock formation 1m away from the BHE

#### 4.4 Long-term performance of the BHE

In order to test the performance of the BHE in “12+12 mode” during the 20-year operation period, analyze the peak and end values (when stop running) of the 150th day of the heating season each year when the inlet temperature is 15°C (as shown in Fig. 15). Fig. 15(a) shows that the heat extraction power decreases year by year. The peak values of the heat extraction power when heating on the 150th day of the 20th year decreased by 13.98%, 14.12% and 14.22% respectively, compared to that of the first year when the inlet temperature is 15°C, 18°C and 20°C. And the end values of that decreased by 14.33 %, 14.45% and 14.56% respectively. Besides, the decline rate is less than 1% after 5 years of the operation.

Similarly, Fig. 15(b) shows that the outlet temperature decreases year by year, but less decline than that of the heat extraction power. The peak values of the outlet temperature when heating on the 150th day of the 20th year decreased by 5.68%, 6.22%

and 7.11% respectively, compared to that of the first year when the inlet temperature is 20°C, 18°C and 15°C. And the end values of that decreased by 3.80 %, 4.35% and 5.28% respectively. Besides, the decline rate is less than 0.5% after 4 years of the operation.

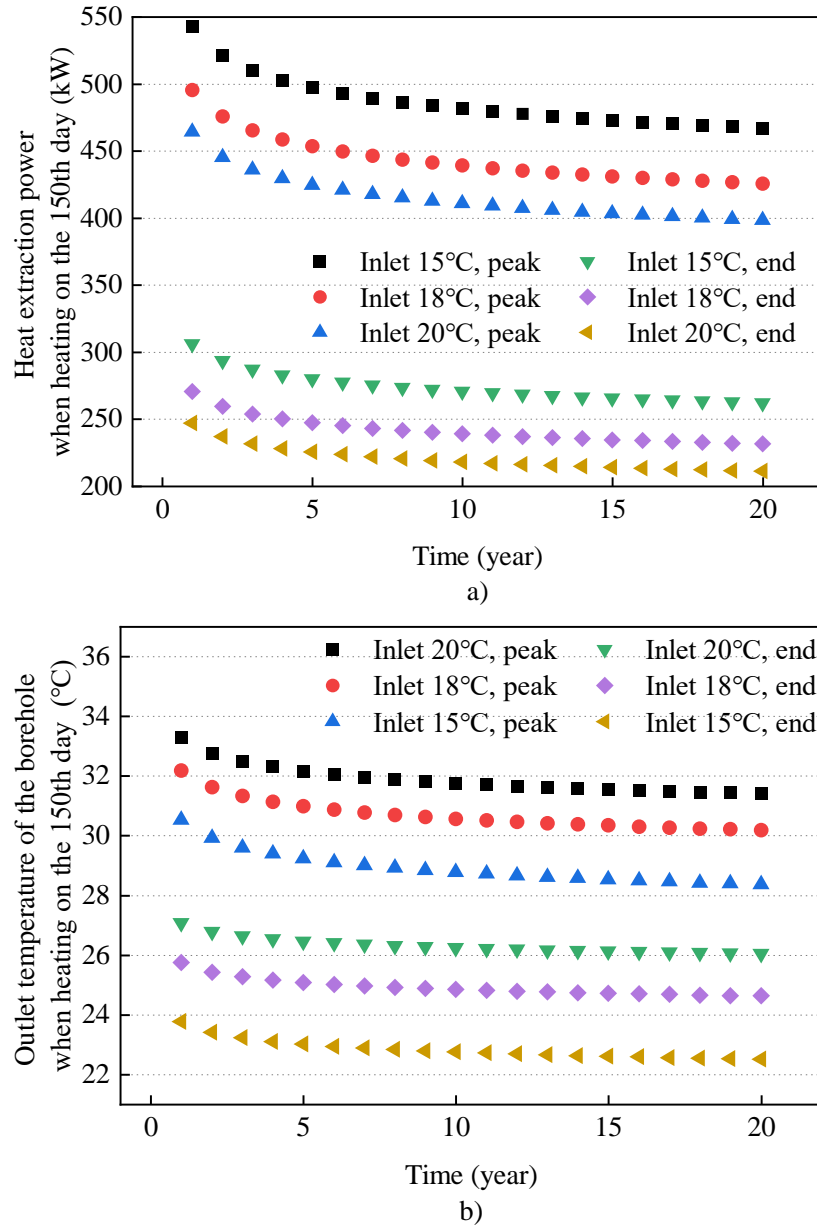


Fig.15 Long-term performance of the BHE

## 5. Conclusions

The numerical model established in this paper for the coaxial deep BHE can accurately reflect the heat transfer process between the BHE and rock formation. The

simulated results were compared with the measured data provided in the literature [32] to verify the accuracy of the model. Compared the performance of the BHE in different operating modes, observed the changes in the temperature distribution of the underground before and after the winter vacation and analyzed long-term performance of the BHE, the following conclusions have been drawn:

- (1) In the 4 operating modes, with the inlet temperature decreasing, the heat extraction power increases. It is better for heat extraction to keep lower inlet fluid temperature to the borehole. Hence, it is proposed to apply a phase change storage tank in geothermal district heating systems[33]. As shown in Fig.16, the tank store excess heat extraction (valves V2 and V4 are open) to maintain inlet fluid temperature within a set range (15-20°C), and it release heat (valves V1 and V3 are closed) as a supplemental heat source for space heating during the shutdown of the underground heat exchanger.

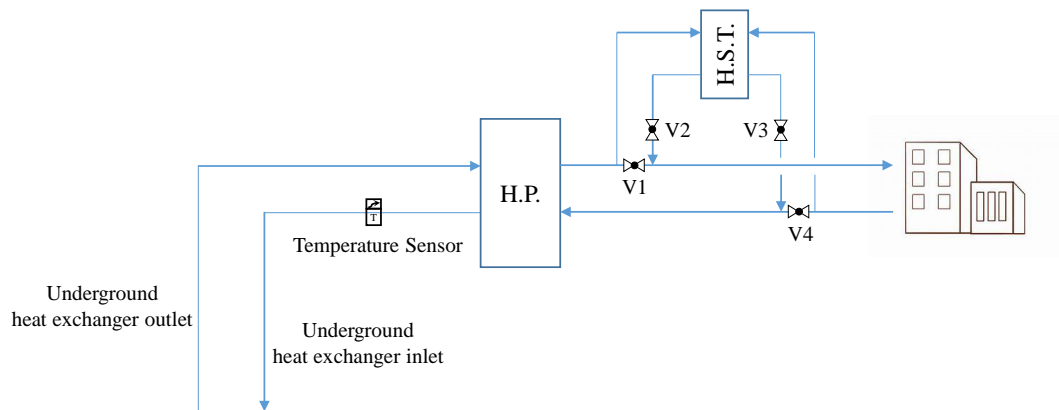


Fig.16 Geothermal district heating system (H.S.T.=Hot Storage Tank, H.P.=Heat Pump)

- (2) Comparison of the four operating strategies of continuous operation, “16+8 mode”, “12+12 mode”, and “8+16 mode” show that when the operation is stable in “12+12 mode”, the heat extraction power can maintain at 301.6 - 528.1kW to cover the

heating load of 4524.00 - 7921.50 m<sup>2</sup> building area in the first year (with the heat pump COP = 5), and the rate of decrease does not exceed 15% within a 20-year operating cycle. This mode is very suitable for buildings such as schools and office buildings where the heat load changes regularly over time.

(3) The annual heat extractions for different operating modes are similar. There is also little difference in the amount of heat extraction by each operation mode throughout the day. Therefore, it can be considered that different operation modes only output almost the same heat in different time periods. In other words, the difference is the heating extraction power. Besides, lowering the inlet temperature has a positive effect on the annual heat extraction, the heat extraction on the 90th day and the heat extraction power.

(4) The temperature distribution of the deeper rock formations is deteriorated more seriously during operation, so its temperature is more difficult to recover. During operation, temperature fluctuations increase with increasing depth. The system stops running after 90 days in the "12+12 mode". Relative to initial temperature of the rock formations, 1 meter away from the center of the BHE, at depths of 500 meters, 1000 meters, 1500 meters, and 2000 meters, the recovery ratios were 90.77%, 82.57%, 79.49%, and 78.37% within 30 days, respectively.

Heat extraction, heat extraction power and the outlet temperature are important performance indicators of the BHE. This paper analyzed the impact on the indicators from the perspective of operating mode and inlet temperature, and provided new ideas for the efficient operation of the BHE. The heat output capability of the borehole heat



exchanger on the 150th day of the 20th year can be utilized as an indicator of the single heat exchange for design calculation.

## **Acknowledgements**

This work was supported by the China National Key R&D Program (Grant No. 2020YFD1100500).

## **References**

- [1] The annual development research report of China building energy conservation, Building energy conservation research center of Tsinghua University, Beijing, 2015.
- [2] J. Li, B.J.J.o.C.P. Shui, A comprehensive analysis of building energy efficiency policies in China: status quo and development perspective, 90 (2015) 326-344.
- [3] Several opinions on promoting the development and utilization of geothermal energy, in: N.E. Administration (Ed.), 2021.
- [4] C. Li, Y. Guan, R. Yang, X. Lu, W. Xiong, A. Long, Effect of inner pipe type on the heat transfer performance of deep-buried coaxial double-pipe heat exchangers, Renewable Energy, 145 (2020) 1049-1060.
- [5] S. Lee, S. Park, M. Kang, H. Choi, Performance evaluation of coaxial-type GHEX in GSHP system installed in Korean residential building, Energy and Buildings, 235 (2021).
- [6] H. Esen, M. Inalli, M. Esen, Technoeconomic appraisal of a ground source heat pump system for a heating season in eastern Turkey, Energy Conversion and Management, 47 (2006) 1281-1297.

- [7] H. Esen, M. Inalli, M. Esen, A techno-economic comparison of ground-coupled and air-coupled heat pump system for space cooling, *Building and Environment*, 42 (2007) 1955-1965.
- [8] H. Esen, M. Inalli, M. Esen, Numerical and experimental analysis of a horizontal ground-coupled heat pump system, *Building and Environment*, 42 (2007) 1126-1134.
- [9] H. Esen, M. Inalli, M. Esen, K. Pihtili, Energy and exergy analysis of a ground-coupled heat pump system with two horizontal ground heat exchangers, *Building and Environment*, 42 (2007) 3606-3615.
- [10] H. Esen, M. Inalli, A. Sengur, M. Esen, Artificial neural networks and adaptive neuro-fuzzy assessments for ground-coupled heat pump system, *Energy and Buildings*, 40 (2008) 1074-1083.
- [11] H. Esen, M. Inalli, A. Sengur, M. Esen, Modeling a ground-coupled heat pump system by a support vector machine, *Renewable Energy*, 33 (2008) 1814-1823.
- [12] H. Esen, M. Inalli, A. Sengur, M. Esen, Modelling a ground-coupled heat pump system using adaptive neuro-fuzzy inference systems, *International Journal of Refrigeration*, 31 (2008) 65-74.
- [13] H. Esen, M. Inalli, A. Sengur, M. Esen, Performance prediction of a ground-coupled heat pump system using artificial neural networks, *Expert Systems with Applications*, 35 (2008) 1940-1948.
- [14] H. Esen, M. Inalli, A. Sengur, M. Esen, Predicting performance of a ground-source heat pump system using fuzzy weighted pre-processing-based ANFIS, *Building and Environment*, 43 (2008) 2178-2187.

- [15] M. Esen, T. Yuksel, Experimental evaluation of using various renewable energy sources for heating a greenhouse, *Energy and Buildings*, 65 (2013) 340-351.
- [16] A. Balbay, M. Esen, Temperature distributions in pavement and bridge slabs heated by using vertical ground-source heat pump systems, *Acta Scientiarum. Technology*, 35 (2013).
- [17] H. Esen, M. Esen, O. Ozsolak, Modelling and experimental performance analysis of solar-assisted ground source heat pump system, *Journal of Experimental & Theoretical Artificial Intelligence* 29 (2017) 1-17.
- [18] M. Esen, Thermal performance of a solar-aided latent heat store used for space heating by heat pump, *Solar Energy*, 69 (2000) 15-25.
- [19] K. Jiao, C. Sun, R. Yang, B. Yu, B. Bai, Long-term heat transfer analysis of deep coaxial borehole heat exchangers via an improved analytical model, *Applied Thermal Engineering*, 197 (2021).
- [20] X. Song, G. Wang, Y. Shi, R. Li, Z. Xu, R. Zheng, Y. Wang, J. Li, Numerical analysis of heat extraction performance of a deep coaxial borehole heat exchanger geothermal system, *Energy*, 164 (2018) 1298-1310.
- [21] C. Wang, Y. Lu, L. Chen, Z. Huang, H. Fang, A semi-analytical model for heat transfer in coaxial borehole heat exchangers, *Geothermics*, 89 (2021).
- [22] P. Li, P. Guan, J. Zheng, B. Dou, H. Tian, X. Duan, H. Liu, Field Test and Numerical Simulation on Heat Transfer Performance of Coaxial Borehole Heat Exchanger, *Energies*, 13 (2020).
- [23] A. Pan, L. Lu, P. Cui, L. Jia, A new analytical heat transfer model for deep borehole

heat exchangers with coaxial tubes, *International Journal of Heat and Mass Transfer*, 141 (2019) 1056-1065.

[24] H. Holmberg, J. Acuña, E. Næss, O.K. Sønju, Thermal evaluation of coaxial deep borehole heat exchangers, *Renewable Energy*, 97 (2016) 65-76.

[25] Z. Wang, F. Wang, J. Liu, Z. Ma, E. Han, M. Song, Field test and numerical investigation on the heat transfer characteristics and optimal design of the heat exchangers of a deep borehole ground source heat pump system, *Energy Conversion and Management*, 153 (2017) 603-615.

[26] L. Fang, N. Diao, Z. Shao, K. Zhu, Z. Fang, A computationally efficient numerical model for heat transfer simulation of deep borehole heat exchangers, *Energy and Buildings*, 167 (2018) 79-88.

[27] J. Liu, F. Wang, W. Cai, Z. Wang, Q. Wei, J. Deng, Numerical study on the effects of design parameters on the heat transfer performance of coaxial deep borehole heat exchanger, *International Journal of Energy Research*, 43 (2019) 6337-6352.

[28] Y. Huang, Y. Zhang, Y. Xie, Y. Zhang, X. Gao, J. Ma, Long-term thermal performance analysis of deep coaxial borehole heat exchanger based on field test, *Journal of Cleaner Production*, 278 (2021).

[29] Y. Luo, J. Yu, T. Yan, L. Zhang, X. Liu, Improved analytical modeling and system performance evaluation of deep coaxial borehole heat exchanger with segmented finite cylinder-source method, *Energy and Buildings*, 212 (2020).

[30] W. Cai, F. Wang, J. Liu, Z. Wang, Z. Ma, Experimental and numerical investigation of heat transfer performance and sustainability of deep borehole heat exchangers

coupled with ground source heat pump systems, *Applied Thermal Engineering*, 149 (2019) 975-986.

[31] J.D. Spitler, S. Javed, R.K. Ramstad, Natural convection in groundwater-filled boreholes used as ground heat exchangers, *Applied Energy*, 164 (2016) 352-365.

[32] K. Morita, W.S. Bollmeier, H. Mizogami, An experiment to prove the concept of the downhole coaxial heat exchanger (DCHE) in Hawaii, (1992).

[33] S.A. Kyriakis, P.L. Younger, Towards the increased utilisation of geothermal energy in a district heating network through the use of a heat storage, *Applied Thermal Engineering*, 94 (2016) 99-110.